

Friedel oscillations and interference patterns from multiple impurities in free fermions in continuous space and in correlated lattice electrons

Banhi Chatterjee,^{1,*} Jan Skolimowski,² and Krzysztof Byczuk³

¹*Institute of Physics, Czech Academy of Sciences, Na Slovance 2, 182 21 Prague, Czech Republic*

²*Scuola Internazionale Superiore di Studi Avanzati (SISSA), Via Bonomea 265, I-34136 Trieste, Italy*

³*Institute of Theoretical Physics, Faculty of Physics, University of Warsaw, ul. Pasteura 5, 02-093 Warszawa, Poland*

(Dated: December 22, 2024)

We study the interference patterns in the Friedel oscillations (FO) due to the scattering off either two or multiple impurities and scattering off extended inhomogeneities both in the non-interacting and two-dimensional lattice systems of interacting fermions. Correlations are accounted for by using an approximate method based on the real-space dynamical mean-field theory. We find that the interference maxima and minima change systematically as we vary the relative distance between the two impurities. At the same time, the interaction increase does not shift the position of interference fringes but only reduces their intensities. A comparison with the single impurity studies clearly shows complex patterns in FO induced by the additional scattering potentials. In the case of an extended step potential the system becomes more homogeneous when the interaction increases. FO and interference patterns are not present in the Mott insulating phase in the single and the many impurity models. Our theoretical study provides promising initial insights and motivate a further realistic modeling to investigate the role of interstitial defects, embedded impurities, ad-atoms on the surfaces, and surface irregularities in materials with different degrees of electronic correlation. For a complete description we also present analytical and numerical results of FO for non-interacting particles moving in a two and three dimensional continuous spaces. In the diluted impurity limit we derive results for FO due to scattering off many impurities, which are generalization of the original Friedel formula.

Keywords: strongly correlated systems, multiple impurity, Friedel oscillations, NRG

I. INTRODUCTION

The presence of an external inhomogeneous potential or defect in metallic systems modulates the electronic charge density around the imperfectness due to the scattering of electrons near the Fermi level. These charge density oscillations are known as the Friedel oscillations (FO) and are mostly visible at low temperatures [1–3]. FO occur in real materials due to the presence of ad-atoms, interstitial defects, or surface irregularities after cleavage. The studies of FO can be significant for a wide range of systems as we discussed in [4–6]. To mention a few, FO have been observed experimentally in quantum corals, metal surfaces like Cu (111), semiconductor surfaces like GaAs (111) around point defects using Scanning Tunneling Microscopy (STM) at around 4–5 K [7–10]. FO have been seen to produce an asymmetry in the quantum transport at the interface of mono-layer and bi-layer graphene which can be used as an application in novel quantum switching devices [11]. It has been demonstrated that the FO, due to the topological defects in the carbon nanotubes, is important for understanding properties like selective dot growth, magnetic interaction through carbon nanotubes and optical spectroscopy of interface states using the tight-binding model [12]. Kolesnychenko *et al.* have observed, using the STM, anisotropic FO while studying the surface electronic structure of transition metal Cr(001) produced by the cleavage of a single crystal

having surface areas, where impurity concentrations slightly exceeded the bulk concentration due to the existence of a high dopant zone in the crystal [13].

In order to theoretically understand the FO in Cr or other transition metals, which belongs to the class of correlated electronic systems, it is important to consider the Coulomb interaction between the electrons. FO have been studied in one-dimensional (1d) interacting fermionic chain using several theories, e.g., the bosonization method or the density-matrix renormalization group [14, 15], or the Bethe-Ansatz local-density approximation [16]. The Fermi liquid theory for two-dimensional (2d) and three-dimensional (3d) systems [17] was applied to investigate FO. The FO induced by non-magnetic impurities in 2d Hubbard model in the presence of interactions have been studied using the slave-boson technique, which involves the static renormalization of the impurity potential [18]. FO seen around the Kondo screening cloud in the presence of magnetic impurities using the t-matrix formalism have been reported in [19].

The dynamical mean-field theory (DMFT) is considered as an advanced and suitable technique to capture the effects of correlations particularly around the Mott metal to insulator transition which is significant for describing the compounds with partially filled d and f shells, e.g., transition metals and their oxides [20–26]. A real space extension of DMFT (R-DMFT) is needed to treat the strongly correlated inhomogeneous systems [27–29].

* banhi.chatterjee@fzu.cz

In our previous work we have investigated the behavior

of FO in models of correlated lattice systems in the metallic and Mott insulating phase in the presence of a single impurity potential using the R-DMFT [4, 6]. We have reported that the oscillations get damped with increasing the interaction, and disappear at the Mott transition and beyond it in the Mott insulating phase.

In reality, a single-site impurity potential could be a too idealized concept when we think of inhomogeneities in the surfaces of true materials. There are usually more than one defects or contamination. Even one encounters extended inhomogeneities and interface effects in multi-layered nano-structures, as for example is discussed in Ref. [30]. Grosu *et al.* studied the problem of FO in 1d noninteracting electron gas in the presence of two impurities, modeled by a double delta function separated by a finite distance, using a linear response theory [31]. They showed that the presence of the second impurity significantly changes the density oscillations (changing the positions of the maxima and minima) depending on the distance between the impurities. The studies of two impurity scattering has been further extended to a 1d interacting fermionic system using the bosonization method in [32]. The scattering and quasiparticle interference from two and multiple magnetic impurities adsorbed on 2d and 3d interacting hosts have been probed using the t-matrix formalism and the numerical renormalization group [33, 34]. However, in these studies the interference effects are discussed in the local density of states in the presence of interactions and not in the particle density oscillations.

We thus see that the studies of FO in the presence of two or multiple impurities have been mostly conducted for the 1d interacting systems, while an attempt to understand real materials requires models in higher dimensions. Moreover, the behavior of FO in the Mott insulating regime for models with many imperfections has not been addressed. Also the current state of knowledge lacks any quantitative treatment of the screening and interference effects in systems in the presence of interactions.

A proper description of FO in real materials with strong electronic correlations demands a realistic modeling combining the density functional theory within the local density approximation and DMFT (LDA+DMFT) [35, 36] and its extension in real space. Such techniques are computationally non-trivial in the presence of inhomogeneities, particularly if it is not just an ad-atom but an impurity atom embedded in the host, e.g. Cr atom in a Pb surface [37]. The translational invariance of the lattice is broken in such a case.

Motivated by the state of art we extend our simple one-band Hubbard model for various types of impurity potentials going beyond the single impurity case and treating the correlations using an approximate self-energy based on DMFT as is discussed in the next Sections. We investigate both non-interacting and

interacting two-dimensional finite lattice systems.

In this paper we address the following questions: (a) How do the FO change due to the interference effects when we introduce the second impurity? (b) How does the interference change when we vary the distance between the impurities and switch on the interaction? (c) How does the picture change if we generalize the two impurities to multiple impurities scattered over the lattice or the extended inhomogeneity? (d) Do we see any interference effect or FO for any of these models of impurity potential in the Mott insulating phase?

Our studies show that the interaction reduces the interference pattern in FO and the screening effects in the system but the interaction does not alter the position of the interference maxima and minima.

Tight-binding models of interacting lattice electrons in two and three dimensions are not tractable on an analytical level. Therefore, to inquire a complete description of the FO in presence of multiple impurities we solve analytically and numerically a model of non-interacting particles moving in a continuous space. We show how presence of few impurities builds interference patterns. In the limit of diluted impurities we derive analytical formulae of the FO in two and three spatial dimensions, which are straightforward generalization of the Friedel result [1–3].

The paper is organized as follows. We start in Sec. II with an analytical and numerical derivation of FO in a non-interacting system in continuous space. Next, we discuss in Sec. III our lattice models and methods used to solve them. We introduce there physical quantities describing our systems. Afterwards in Sec. IV we present our numerical results for: (a) two impurities, (b) multiple impurities, (c) extended inhomogeneity, and (d) a chain of impurities or a domain wall. Finally, in Sec. V we conclude our results and provide an outlook.

II. MULTIPLE IMPURITIES IN NON-INTERACTING SYSTEMS

Before we discuss our results on FO in interacting lattice fermions with multiple impurities we present the corresponding theory for non-interacting particles in continuous space.

A. Exact formal solution

Such a system is described by the Green's function [38]

$$G(\mathbf{r}, \mathbf{r}'; \omega) = \langle \mathbf{r} | \frac{1}{\hbar\omega + i0^+ - \hat{H}} | \mathbf{r}' \rangle, \quad (1)$$

where $\hbar\omega$ is the real energy (\hbar is the Planck constant) and the one particle Hamiltonian is

$$\hat{H} = -\frac{\hbar^2}{2m}\nabla^2 + V(\mathbf{r}), \quad (2)$$

which contains a potential

$$V(\mathbf{r}) = \sum_{i=1}^{N_{\text{imp}}} V_i(\mathbf{r} - \mathbf{l}_i) \quad (3)$$

originated from N_{imp} independent impurities located at positions \mathbf{l}_i . The vector \mathbf{r} is the position variable and m is the particle mass. In this Section all d-dimensional vectors are denoted in boldface. It is known that the Green's function in the presence of an external potential $V(\mathbf{r})$ obeys an integral equation [38]

$$G(\mathbf{r}, \mathbf{r}'; \omega) = G_0(\mathbf{r} - \mathbf{r}'; \omega) + \int dr'' G_0(\mathbf{r} - \mathbf{r}''; \omega) V(\mathbf{r}'') G(\mathbf{r}'', \mathbf{r}'; \omega), \quad (4)$$

where $G_0(\mathbf{r} - \mathbf{r}'; \omega)$ is the Green's function in the continuous space. It takes the form [38]

$$G_0(\mathbf{r} - \mathbf{r}'; \omega) = \begin{cases} -\frac{2m}{\hbar^2} \frac{i}{4} H_0^+(k|\mathbf{r} - \mathbf{r}'|) & \text{for } d = 2 \\ -\frac{2m}{\hbar^2} \frac{e^{ik|\mathbf{r} - \mathbf{r}'|}}{4\pi|\mathbf{r} - \mathbf{r}'|} & \text{for } d = 3, \end{cases} \quad (5)$$

where $k = \sqrt{2m\omega}/\hbar$ and H_0^+ is the 0th order Hankel function. We note that the Green's functions are singular when $|\mathbf{r} - \mathbf{r}'| \rightarrow 0$.

Typically, the impurity potentials $V_i(\mathbf{r})$ in Eq. (3) are short range. Therefore, we model them by a zero-range potential represented by a Dirac-delta function with the strength proportional to the effective scattering strength a_i^s . However, such an extremely localized potential must be properly regularized giving rise to the Fermi pseudopotential [39] with a general form

$$V(\mathbf{r}) = \sum_{i=1}^{N_{\text{imp}}} a_i^s \delta(\mathbf{r} - \mathbf{l}_i) \hat{\mathcal{R}}_d, \quad (6)$$

where $\hat{\mathcal{R}}_d$ is a regularization operator depending on system dimensionality [40–42]. E.g., in three dimensions $\hat{\mathcal{R}}_d = 4\pi(\partial/\partial r)r$ [40–42]. The pseudopotential mimics the fact that the wave function is strongly suppressed inside the impurity potential. On the other hand, the regularization $\hat{\mathcal{R}}_d$ allows to avoid a singular behavior of the Green's functions when $|\mathbf{r} - \mathbf{r}'| \rightarrow 0$. One should also note that in dimensions higher than one a pure Dirac-delta like potential is invisible to particles, which means that they are not scattered at all. The use of the Fermi pseudopotential allows us to deal with a zero-range potential but which still has scattering effects. In the following we write

$$V(\mathbf{r}) = \sum_{i=1}^{N_{\text{imp}}} V_i \delta(\mathbf{r} - \mathbf{l}_i), \quad (7)$$

where V_i parameters as well as the Green's function $G_0(\mathbf{0}; \omega)$ are supposed to be adequately renormalized quantities [40–42].

For a system with local impurity potentials the integral equation reads

$$G(\mathbf{r}, \mathbf{r}'; \omega) = G_0(\mathbf{r} - \mathbf{r}'; \omega) + \sum_{i=1}^{N_{\text{imp}}} V_i G_0(\mathbf{r} - \mathbf{l}_i; \omega) G(\mathbf{l}_i, \mathbf{r}'; \omega), \quad (8)$$

Expressing the left hand side at $\mathbf{r} = \mathbf{l}_i$ we obtain a set of linear equations to determine $G(\mathbf{l}_i, \mathbf{r}'; \omega)$, i.e.

$$G(\mathbf{l}_i, \mathbf{r}'; \omega) = G_0(\mathbf{l}_i - \mathbf{r}'; \omega) + \sum_{j=1}^{N_{\text{imp}}} V_j G_0(\mathbf{l}_i - \mathbf{l}_j; \omega) G(\mathbf{l}_j, \mathbf{r}'; \omega). \quad (9)$$

This set of equations can be written in a matrix form

$$\sum_{j=1}^{N_{\text{imp}}} M_{ij}(\omega) G(\mathbf{l}_j, \mathbf{r}'; \omega) = G_0(\mathbf{l}_i - \mathbf{r}'; \omega), \quad (10)$$

where the M matrix is

$$M_{ij}(\omega) = [\delta_{ij} - V_j G_0(\mathbf{l}_i - \mathbf{l}_j; \omega)]. \quad (11)$$

The diagonal elements of this matrix $M_{ii}(\omega) = [1 - V_i G_0(\mathbf{0}; \omega)]$ are not singular due to a regularization procedure [40–42]. Then, by inverting this matrix, in the absence of bound states, either analytically or numerically for each ω we find the solution of Eq. (9)

$$G(\mathbf{l}_i, \mathbf{r}'; \omega) = \sum_{j=1}^{N_{\text{imp}}} M_{ij}^{-1}(\omega) G_0(\mathbf{l}_j - \mathbf{r}'; \omega). \quad (12)$$

Finally, by using Eq. (8) we determine the exact Green's function

$$G(\mathbf{r}, \mathbf{r}'; \omega) = G_0(\mathbf{r} - \mathbf{r}'; \omega) + \sum_{i,j=1}^{N_{\text{imp}}} G_0(\mathbf{r} - \mathbf{l}_i; \omega) T_{ij}(\omega) G_0(\mathbf{l}_j - \mathbf{r}'; \omega), \quad (13)$$

where

$$T_{ij}(\omega) = V_i M_{ij}^{-1}(\omega) \quad (14)$$

is a t-matrix. The local density of states (LDOS) is provided by the diagonal part of the Green's function

$$\rho(\mathbf{r}; \omega) = -\frac{1}{\pi} \text{Im} G(\mathbf{r}, \mathbf{r}; \omega), \quad (15)$$

and the local density of non-interacting fermions at $T = 0$ with the Fermi energy E_F is given by

$$n(\mathbf{r}) = \int_0^{E_F} d\omega \rho(\mathbf{r}; \omega) = -\frac{1}{\pi} \int_0^{E_F} d\omega \text{Im} G(\mathbf{r}, \mathbf{r}; \omega). \quad (16)$$

It is clear that in the multiple impurity case, the terms $G_0(\mathbf{r}-\mathbf{l}_i;\omega)G_0(\mathbf{l}_j-\mathbf{r};\omega)$ are responsible for an oscillatory behavior with respect to \mathbf{r} of the LDOS and the charge density. Note that in this Sec. II we neglect for simplicity the spin of particles, which otherwise would lead to a trivial factor of two in the corresponding equations.

B. Explicit analytical and numerical solutions in special cases

For a small number of scattering centers one can invert the matrix M analytically.

1. A single impurity

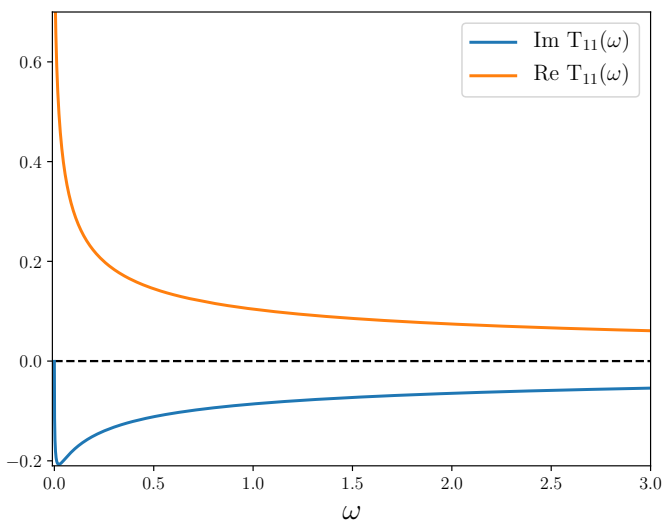


FIG. 1. The real and imaginary part of the t-matrix for a single impurity with $V_1 = 1$.

For example, for $N_{\text{imp}} = 1$ we find that $M_{11}(\omega) = 1 - V_1 G_0(\mathbf{0};\omega)$ and therefore

$$G(\mathbf{r}, \mathbf{r}'; \omega) = G_0(\mathbf{r} - \mathbf{r}'; \omega) + G_0(\mathbf{r} - \mathbf{l}_1; \omega) T_{11}(\omega) G_0(\mathbf{l}_1 - \mathbf{r}'; \omega), \quad (17)$$

where

$$T_{11}(\omega) = \frac{V_1}{1 - V_1 G_0(\mathbf{0}; \omega)}. \quad (18)$$

In Fig. 1 we present the real and imaginary parts of the t-matrix for the single impurity with $V_1 = 1$ in three dimensions. Here in Sec. II B we have used units with $2m/\hbar^2 = 1$. The Fermi energy E_F is fixed by demanding that the uniform particle density is equal to one.

The changes in the local density of particles is determined

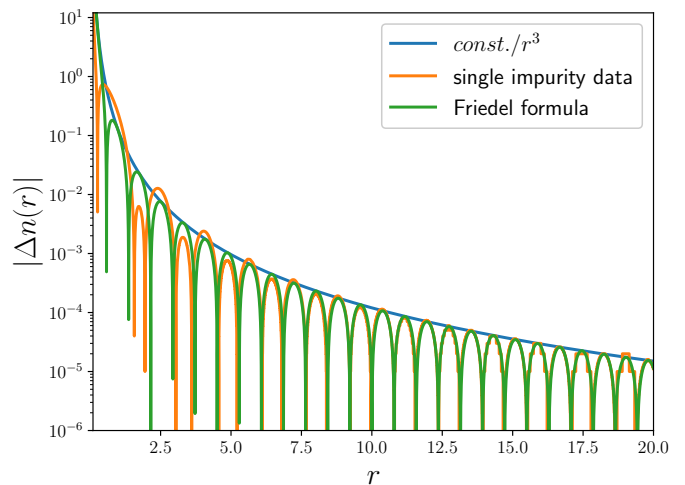


FIG. 2. Friedel oscillations due to a single impurity with $V_1 = 1$ in three dimensions. The orange curve represents the exact result determined with using the t-matrix (18). The blue curve shows the behavior of the envelope which asymptotically decays with a distance as $1/r^3$ (the constant is 0.15). The green curve represents oscillatory behavior derived from the asymptotic Friedel formula (20).

by

$$\Delta n(\mathbf{r}) = -\frac{1}{\pi} \int_0^{E_F} d\omega \text{Im} G_0(\mathbf{r}; \omega) T_{11}(\omega) G_0(-\mathbf{r}; \omega). \quad (19)$$

In Fig. 2 we present the exact result for the changes of the particle densities from the potential located at the origin $\mathbf{l} = 0$. The stepwise behavior at large r is due to a finite numerical accuracy in determining the integrals. It can be easily verified that at large distances the amplitudes of the oscillation decay as $1/r^3$, which is described by the original Friedel formula in three dimensions, namely

$$\Delta n(\mathbf{r}) = I^s \frac{\cos(2k_F r + \phi_s)}{r^3}, \quad (20)$$

where $k_F = \sqrt{2mE_F}/\hbar$ is the Fermi vector length, $r = |\mathbf{r}|$, ϕ_s is a phase shift, and I^s is the constant proportional to the effective scattering length [43]. In deriving the Eq. (20) the ω -dependence of the t-matrix is neglected and it is approximated by its value in the $k \rightarrow 0$ limit. In Fig. 2 we plot the density changes determined from the asymptotic Friedel formula (20) and we see that at distances $r \gtrsim 7$ it practically gives the same results as those obtained exactly.

2. Two impurities

For $N_{\text{imp}} = 2$ we find that

$$\begin{aligned}
G(\mathbf{r}, \mathbf{r}'; \omega) &= G_0(\mathbf{r} - \mathbf{r}'; \omega) \\
&+ G_0(\mathbf{r} - \mathbf{l}_1; \omega) T_{11}(\omega) G_0(\mathbf{l}_1 - \mathbf{r}'; \omega) \\
&+ G_0(\mathbf{r} - \mathbf{l}_1; \omega) T_{12}(\omega) G_0(\mathbf{l}_2 - \mathbf{r}'; \omega) \\
&+ G_0(\mathbf{r} - \mathbf{l}_2; \omega) T_{21}(\omega) G_0(\mathbf{l}_1 - \mathbf{r}'; \omega) \\
&+ G_0(\mathbf{r} - \mathbf{l}_2; \omega) T_{22}(\omega) G_0(\mathbf{l}_2 - \mathbf{r}'; \omega), \quad (21)
\end{aligned}$$

where

$$T_{11}(\omega) = \frac{V_1}{[1 - V_1 G_0(\mathbf{0}; \omega)][1 - V_2 G_0(\mathbf{0}; \omega)] - V_1 V_2 G_0(\mathbf{l}_1 - \mathbf{l}_2; \omega) G_0(\mathbf{l}_2 - \mathbf{l}_1; \omega)} [1 - V_2 G_0(\mathbf{0}; \omega)], \quad (22)$$

$$T_{12}(\omega) = \frac{V_1}{[1 - V_1 G_0(\mathbf{0}; \omega)][1 - V_2 G_0(\mathbf{0}; \omega)] - V_1 V_2 G_0(\mathbf{l}_1 - \mathbf{l}_2; \omega) G_0(\mathbf{l}_2 - \mathbf{l}_1; \omega)} V_2 G_0(\mathbf{l}_1 - \mathbf{l}_2; \omega), \quad (23)$$

$$T_{21}(\omega) = \frac{V_2}{[1 - V_1 G_0(\mathbf{0}; \omega)][1 - V_2 G_0(\mathbf{0}; \omega)] - V_1 V_2 G_0(\mathbf{l}_1 - \mathbf{l}_2; \omega) G_0(\mathbf{l}_2 - \mathbf{l}_1; \omega)} V_1 G_0(\mathbf{l}_2 - \mathbf{l}_1; \omega), \quad (24)$$

and

$$T_{22}(\omega) = \frac{V_2}{[1 - V_1 G_0(\mathbf{0}; \omega)][1 - V_2 G_0(\mathbf{0}; \omega)] - V_1 V_2 G_0(\mathbf{l}_1 - \mathbf{l}_2; \omega) G_0(\mathbf{l}_2 - \mathbf{l}_1; \omega)} [1 - V_1 G_0(\mathbf{0}; \omega)]. \quad (25)$$

Due to the multiple scattering between the two impurities the t-matrix is not a sum of t-matrices for two independent impurities located at different points. It is a matrix element function which depends only on the energy ω and a distance between the impurities $\Delta l = |\mathbf{l}_1 - \mathbf{l}_2|$.

In Fig. 3 we plot the real and imaginary parts of the off-diagonal t-matrix elements for different distances between the impurities in three dimensions. For comparison we also present the ratios of real and imaginary parts between off-diagonal and diagonal matrix elements. Because of the inter-impurity scattering and interferences of quantum waves the t-matrix oscillates and changes a sign in contrast to the single impurity case in Fig. 1. Moreover, we can see that with increasing the inter-impurity distance the relative values of the off-diagonal elements with respect to the diagonal elements are decreasing.

In Fig. 4 we present exact results for FO in case of two impurities in three dimensions at different distances Δl . A strong interference oscillations are visible between the impurities. Outside them the oscillation amplitudes decay as $1/r^3$, similarly as in one impurity case. We also plot in Fig. 4 the results when the off-diagonal t-matrix elements are neglected. Differences are very small and mostly visible in space between the impurities. Outside them the results depicted by blue (exact) and orange

(approximate) lines are almost the same.

For $N_{\text{imp}} = 3$ or 4 it is still possible to invert the matrix M analytically and obtain the exact analytical expressions for the Green's functions. This allows to investigate FO in analytical details. However, the final equations become more and more cumbersome, cf. [41].

C. Approximation in diluted impurity limit and generalized Friedel formula

An important simplification occurs when the impurities are far away from each other, i.e., $|\mathbf{l}_i - \mathbf{l}_j|$ is large as compared to other relevant distances, e.g., the Fermi wave length. In this diluted limit we can neglect the off diagonal elements of the matrix M because the Green's function decays as $G_0(\mathbf{l}_i - \mathbf{l}_j; \omega) \sim 1/|\mathbf{l}_i - \mathbf{l}_j|^{(d-1)/2}$, cf. Fig. 3. In this limit

$$M_{ij}^{-1}(\omega) = \frac{\delta_{ij}}{1 - V_i G_0(\mathbf{0}; \omega)} \quad (26)$$

and

$$T_{ij}(\omega) = \delta_{ij} \frac{V_i}{1 - V_i G_0(\mathbf{0}; \omega)}. \quad (27)$$

The t-matrix is diagonal and each matrix element takes into account only multiple scattering on the corresponding single impurity. Inter-impurity scattering effects are

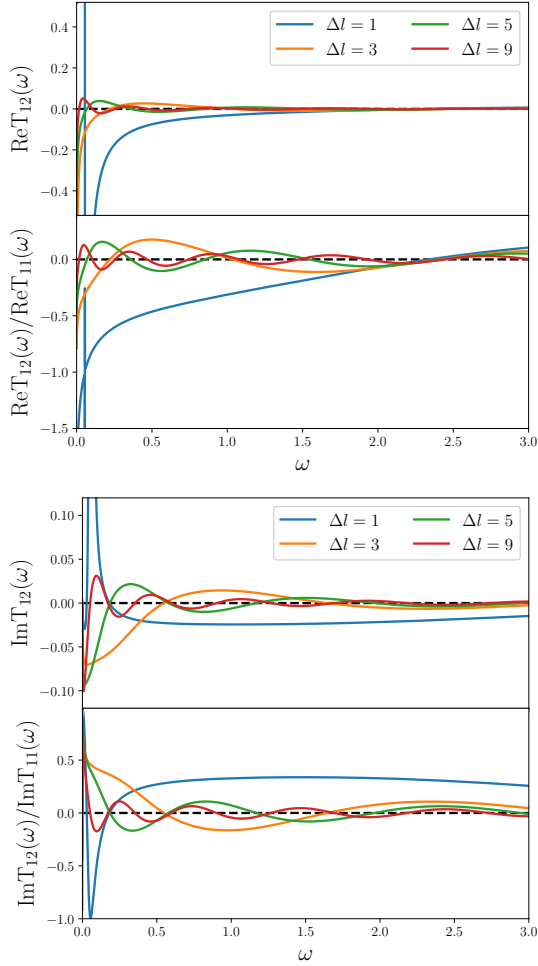


FIG. 3. Real (upper panel) and imaginary (lower panel) of the off-diagonal t-matrix elements and their ratio with respect to diagonal elements for different distances between impurities with $V_1 = V_2 = 1$ in three dimensions.

neglected in this limit. The Green's function is now given by

$$G(\mathbf{r}, \mathbf{r}'; \omega) = G_0(\mathbf{r} - \mathbf{r}'; \omega) + \sum_{i=1}^{N_{\text{imp}}} G_0(\mathbf{r} - \mathbf{l}_i; \omega) T_{ii}(\omega) G_0(\mathbf{l}_i - \mathbf{r}'; \omega), \quad (28)$$

and changes due to multiple impurities in the LDOS is

$$\Delta\rho(\mathbf{r}; \omega) = -\frac{1}{\pi} \sum_{i=1}^{N_{\text{imp}}} \text{Im} G_0(\mathbf{r} - \mathbf{l}_i; \omega) T_{ii}(\omega) G_0(\mathbf{l}_i - \mathbf{r}; \omega). \quad (29)$$

Finally, the changes in the local density is determined from

$$\Delta n(\mathbf{r}) = -\frac{1}{\pi} \sum_{i=1}^{N_{\text{imp}}} \int_0^{E_F} d\omega \text{Im} G_0(\mathbf{r} - \mathbf{l}_i; \omega) T_{ii}(\omega) G_0(\mathbf{l}_i - \mathbf{r}; \omega). \quad (30)$$

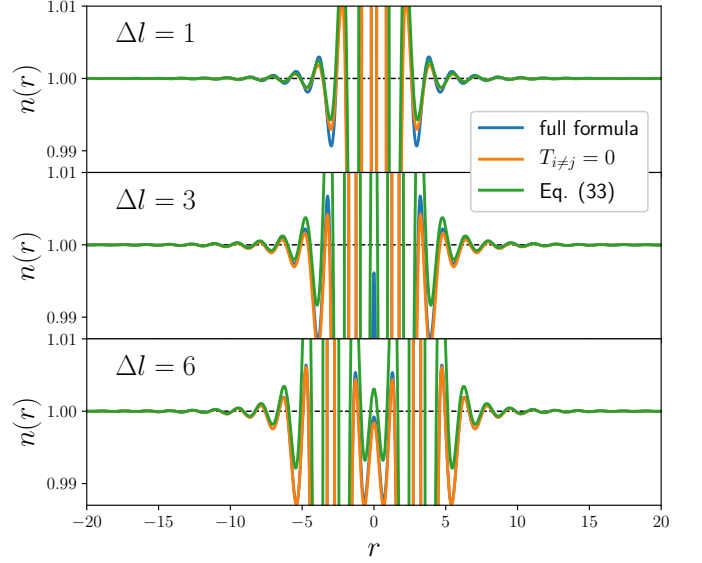


FIG. 4. Friedel oscillations due to two impurities with $V_1 = V_2 = 1$ at different distances Δl in three dimensions. The blue curves represent the exact result determined with using the t-matrix Eqs. (22-25). The orange curves show the behavior of the Friedel oscillations when the off-diagonal elements of t-matrix are neglected. The green curves represent oscillatory behavior derived from the generalized Friedel formula (33).

In the limit of diluted impurities the FO pattern is a sum of FO patterns coming from each scattering centers independently.

Using an explicit form of the Green's function in three dimensions (Eq. 5) and approximating the t-matrix by an effective scattering length

$$b_i^s = \lim_{k \rightarrow 0} f^+(k), \quad (31)$$

where $\hbar\omega = \hbar^2 k^2 / 2m$ and $f^+(k)$ is the scattering amplitude due to the i -th impurity and obtained directly from the t-matrix $T_{ii}(\omega)$ we find that the change in the particle density is expressed by

$$\Delta n(\mathbf{r}) = \sum_{i=1}^{N_{\text{imp}}} I_i^s \frac{(2k_F |\mathbf{r} - \mathbf{l}_i|) \cos(2k_F |\mathbf{r} - \mathbf{l}_i|) - \sin(2k_F |\mathbf{r} - \mathbf{l}_i|)}{(2k_F |\mathbf{r} - \mathbf{l}_i|)^4}, \quad (32)$$

where $I_i^s \sim b_i^s$ are constants depending on the impurity potential strengths V_i [43]. In the asymptotic limit $|\mathbf{r} - \mathbf{l}_i| \gg 1/k_F$ we obtain a generalization of the Friedel result to multiple impurity case

$$\Delta n(\mathbf{r}) = \sum_{i=1}^{N_{\text{imp}}} I_i^s \frac{\cos(2k_F |\mathbf{r} - \mathbf{l}_i|)}{(2k_F |\mathbf{r} - \mathbf{l}_i|)^3}. \quad (33)$$

In the dilute limit one expects that FO pattern is a sum of FO patterns yielded by each independent impurity. The oscillatory behavior decays as the cubic distance

from the impurities. In Fig. 4 we plot the results for FO based on the generalized formula (33) in case of two impurities in three dimensions and compare them with the exact results. The ω -dependence of the diagonal t-matrix elements seems to be relevant is space between the impurities. However, outside the impurities the Eq. (33) practically describes the FO of two impurities very well.

In a similar way one can obtain the generalization of Friedel result in two dimensions

$$\Delta n(\mathbf{r}) = \sum_{i=1}^{N_{\text{imp}}} I_i^s \frac{\sin(2k_F|\mathbf{r} - \mathbf{l}_i| + \phi_i)}{(2k_F|\mathbf{r} - \mathbf{l}_i|)^2}, \quad (34)$$

where ϕ_i are certain phase shifts. The last result required an asymptotic form of the Green's function in two dimension, which is found from an asymptotic expansion of the Hankle function $H_j^+(z) \approx \sqrt{2/\pi z} \exp[i(z - (2\nu + 1)\pi/4)]$. The oscillatory behavior decays as the square distance from the impurities.

Finally we note that a superposition of FO from independent impurities gives rise to interference patterns. Few cases, determined from Eq. (34) for multiple impurities in two dimensions, are shown in Fig. 5. We selected the phase shifts $\phi_i = 0$ for each impurities and $k_F = 1$, which sets a characteristic wave-length scale $\lambda_F = 2\pi/k_F$. Hence, the uniform density of particles is different from that in Sec. II B. The presented patterns resemble those seen in various STM experiments on metallic surfaces with defects or impurities.

III. MODEL AND METHOD

In order to demonstrate a role of strong correlations between the electrons we consider a lattice model with on-site inter-particle interaction. Such a system is described by the Hubbard model. With changing the inter-particle interaction strength the system described by this model evolves between the Fermi liquid regime and the Mott insulator regime. In the rest of the paper we present FO interference patterns in these different regimes. The very first difference with respect to continuous case, presented earlier, is a lack of rotational symmetry. In addition the continuous case is not able to describe the Mott insulating phase and the metal-insulator transition, which are indications of strong correlations.

A. Model

We consider the one-band Hubbard model [44–46] with an external inhomogeneous potential

$$H = \sum_{ij,\sigma} t_{ij} \hat{a}_{i\sigma}^\dagger \hat{a}_{j\sigma} + \sum_{i\sigma} V_{i\sigma} \hat{a}_{i\sigma}^\dagger \hat{a}_{i\sigma} + U \sum_i \hat{n}_{i\downarrow} \hat{n}_{i\uparrow}, \quad (35)$$

where $\hat{a}_{i\sigma}$ ($\hat{a}_{i\sigma}^\dagger$) is the annihilation (creation) fermionic operator with spin σ on the i^{th} lattice site, t_{ij} is the hopping matrix element between the i^{th} and j^{th} sites with $t_{ii} = 0$. The second term describes the external (inhomogeneous) potential given by $V_{i\sigma}$ which is assumed to be real. The third term models the local part of the electronic interaction between two fermions with opposite spins located on the same lattice site.

We consider a two dimensional square lattice with the number of lattice sites $N_L = 31^2$ (the size of the lattice is 31×31) and the following models of the external (inhomogeneous) spin independent potential:

- Two single site impurities placed either along the diagonal direction of the lattice or along a vertical direction of the lattice for different relative distances. Mathematically, $V_i = V_{01}\delta_{ii_{01}} + V_{02}\delta_{ii_{02}}$.
- A more general case where several impurities are randomly scattered over various lattice sites. This aims to model a contaminated surface with various dopant zones or interstitial defects. Mathematically, $V_i = V_{01}\delta_{ii_{01}} + V_{02}\delta_{ii_{02}} + V_{03}\delta_{ii_{03}} + \dots$
- A step like potential or extended inhomogeneity across the lattice aimed to describe inhomogeneous surface irregularities after a cleavage. Mathematically, $V_{i\sigma} = V_0\Theta(X_i - X_0)$, where X_0 is the horizontal lattice coordinate where the steplike potential begins (i.e., the Heaviside function $\Theta(x)$ is non-zero).
- A chain of impurities placed along the diagonal and vertical directions of the lattice aimed to model a domain wall or an interface. In freshly cleaved samples such domain walls can be found connecting large lattice inhomogeneties and can be observed experimentally using the STM.

B. Method

All single particle properties of the system are obtained from the retarded Green's function obtained by inverting the matrix Dyson equation [47] in the lattice position space

$$\mathbf{G}(z) = [(z + \mu)\mathbf{1} - \mathbf{t} - \mathbf{V} - \Sigma(z)\mathbf{1}]^{-1}, \quad (36)$$

where $\hbar z = \omega + i0^+$ is the energy approaching the real axis from above and μ is the chemical potential. $\Sigma(z)$ is the site independent homogeneous part of the self-energy which approximates the effect of correlations and is calculated using the DMFT for the same parameters of the corresponding homogeneous Hubbard Hamiltonian. Hereafter, all matrices are expressed in bold faced notation. The non-diagonal matrix \mathbf{t} corresponds to the hopping amplitudes t_{ij} and the diagonal matrix \mathbf{V} reflects the on-site inhomogeneous potential V_i . The unity matrix is written as $\mathbf{1}$.

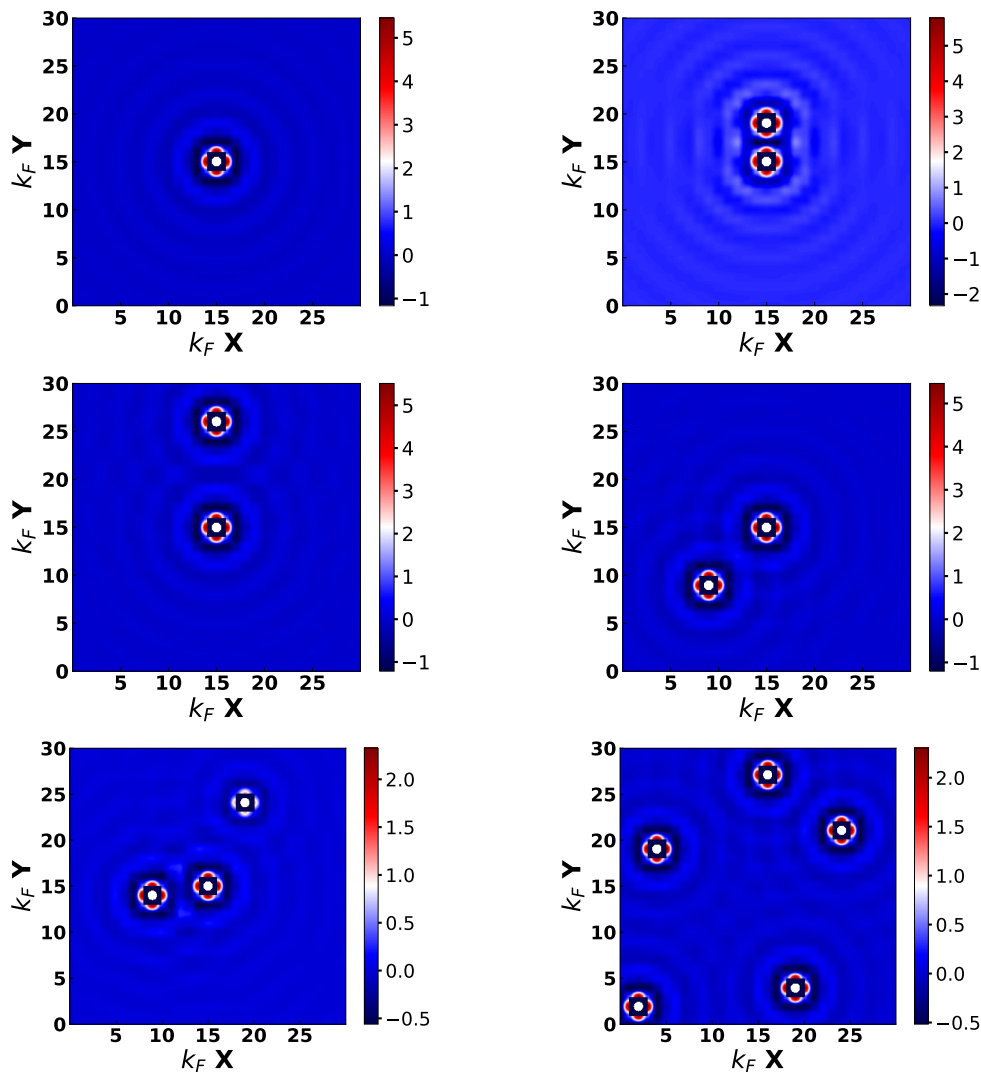


FIG. 5. Friedel oscillations and interference patterns in two dimensional system of non-interacting fermions. Upper left panel: A single impurity with $I_1 = 24$ placed at $\mathbf{l}_1 = (16, 16)$. Upper right panel: Two impurities close to each other with $I_1 = I_2 = 24$ placed at $\mathbf{l}_1 = (16, 16)$ and $\mathbf{l}_2 = (16, 20)$. Middle left panel: Two impurities far away from each other with $I_1 = I_2 = 24$ placed at $\mathbf{l}_1 = (16, 16)$ and $\mathbf{l}_2 = (16, 27)$. Middle right panel: Two impurities placed diagonally with $I_1 = I_2 = 24$ placed at $\mathbf{l}_1 = (10, 10)$ and $\mathbf{l}_2 = (16, 16)$. Lower left panel: Three impurities with different strengths $I_1 = 10$ at $\mathbf{l}_1 = (16, 16)$, $I_2 = 10$ at $\mathbf{l}_1 = (10, 15)$, and $I_3 = 5$ at $\mathbf{l}_1 = (20, 25)$. Lower right panel: Multiple impurities with $I_i = 5$ and at positions $\mathbf{l}_1 = (3, 3)$, $\mathbf{l}_2 = (20, 5)$, $\mathbf{l}_3 = (5, 20)$, $\mathbf{l}_4 = (25, 22)$, and $\mathbf{l}_5 = (17, 28)$. Here, the uniform density of particles is set by $k_F = 1$, which leads to a characteristic wave-length scale $\lambda_F = 2\pi/k_F$.

In the DMFT the self-energy is diagonal in lattice site indices and accounts for all local dynamic correlation effects. In case of homogeneous lattice systems, all lattice sites are equivalent. The self-energy is computed by mapping a lattice site into an effective single impurity Anderson model (SIAM) and solving it by using standard techniques like a continuous time quantum Monte Carlo, an exact diagonalization, a numerical renormalization group method (NRG), etc. However, in the presence of external impurities, translational invariance of the lattice is broken and the lattice sites are non-equivalent. Hence, it is essential now to solve the SIAM separately at each lattice site and the local self-energy becomes site dependent. In other words, in an inhomogeneous system the self-energy has a homogeneous part due to

the electron-electron interactions and an inhomogeneous part due to the contribution from the interaction and the external impurities. Owing to the site dependent part of the self-energy, the result of the impurity potential in the system is not static but effectively dynamic [5]. Ideally, in order to get the full picture of a correlated inhomogeneous system we should consider both the homogeneous and inhomogeneous part of the self energy solving the full real-space DMFT (R-DMFT) equations self-consistently.

Unfortunately, deciphering the full R-DMFT equations is computationally exhaustive, especially for higher-dimensional systems with a large number of lattice sites. Hence, as a first approximation we omit the

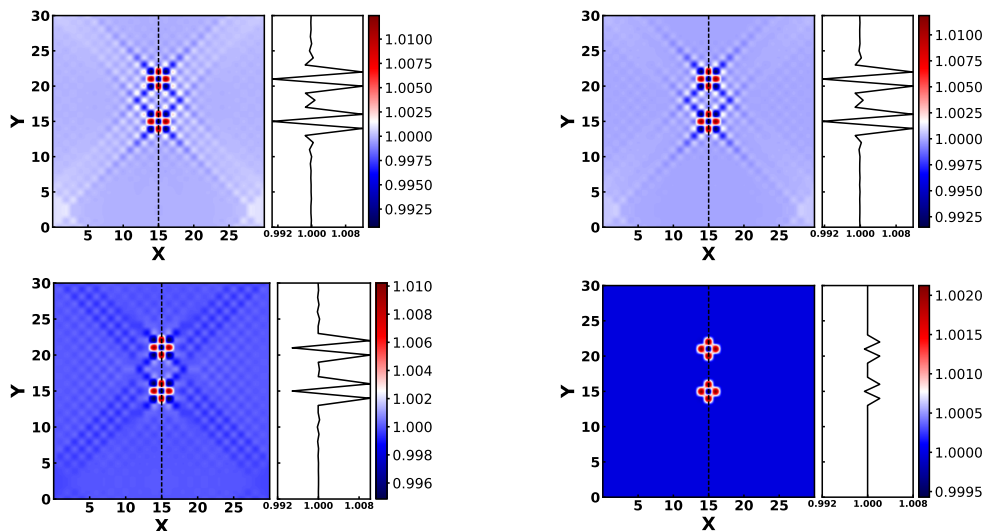


FIG. 6. Interference effect on FO due to the scattering from two impurities of equal magnitude, i.e. $V_{01} = V_{02} = 24t$ placed at $\vec{R}_{01} = (15a, 15a)$ and $\vec{R}_{02} = (15a, 22a)$ respectively along the vertical direction of the (31×31) square lattice. We show $U = 0t, 2t$ (upper panel, left to right) $5t, 12t$ (lower panel, left to right). The insets (on the right) show oscillations along the vertical line passing through the impurities. The color scale is spanned in between the highest and lowest values of the density in the system. The color scale changes for different U since the minimal value of the density increases with it.

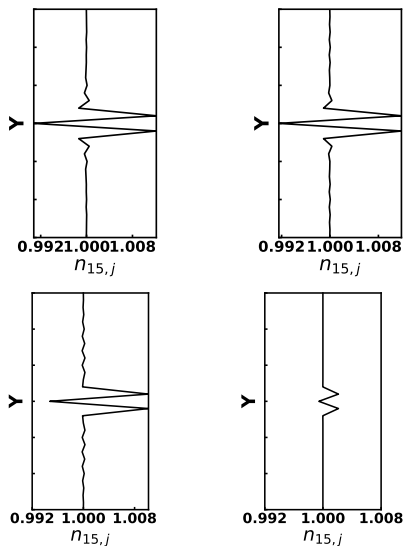


FIG. 7. FO in the square lattice in the presence of a single impurity $V_0 = 24t$ in the centre ($\vec{R}_0 = (15a, 15a)$). All other model parameters and plotting style is the same as in Fig. 6. We show $U = 0t, 2t$ (upper panel, left to right) and $5t, 12t$, (lower panel, left to right). We only show the vertical line passing through site containing the impurity for a comparison with Fig 6. A complete density profile for the single impurity case is available in [6].

inclusion of inhomogeneous, site-dependent part of the self-energy in our present studies to obtain some initial insights on the behavior of the system with correlations. We call this approximation homogeneous self-energy approximation (HSEA) [6]. The homogeneous part of the self-energy is computed by solving the DMFT self-consistency equations for infinite homogeneous

system at zero temperature by using the NRG method. The open-source code “NRG Ljubljana” [49, 50] is used for this purpose. The computed self-energy (within the HSEA) is then transferred to the real space Dyson equation (36) containing the impurity potential and used to obtain the one-particle Green’s function. We note here that although the self-energies are computed for a homogeneous system, the Green’s function is still obtained by inverting the Dyson equation containing the impurity potential in the real space and thus inhomogeneity of the system is taken into account.

A detailed mathematical formalism of the R-DMFT and HSEA is presented in [6] wherein we also show that the results from the two methods agree well for a single impurity potential. It might be an interesting future project to compare the results from R-DMFT and HSEA for our extended models of the impurity potentials.

C. Physical quantities

Once we know the Green’s function of the system from Eq. (35) and (36) we obtain the local spectral function as

$$A_{i\sigma}(\omega) = -\frac{1}{\pi} \text{Im} G_{ii\sigma}(\omega). \quad (37)$$

Having (37) we compute the spin resolved local density of particles at zero temperature as

$$\bar{n}_{i\sigma} = \int_{-\infty}^{E_F} A_{i\sigma}(\omega) f(\omega) d\omega. \quad (38)$$

We consider spin rotational invariant systems, i.e., $\bar{n}_{i\uparrow} = \bar{n}_{i\downarrow}$, and the total number of particles per site is given by

$$\bar{n} = \frac{1}{N_L} \sum_{i=1}^{N_L} \bar{n}_i, \quad (39)$$

where $\bar{n}_i = n_{i\uparrow} + n_{i\downarrow}$. Eq. (38) is the most relevant for our studies of FO.

We further quantify the screening and interference effects in the system by the screening charge defined by

$$Z = \sum_{i\sigma} \left(\bar{n}_{i\sigma} - \frac{\bar{n}_{\text{hom}}}{2} \right), \quad (40)$$

where the summation runs over all the lattice sites and \bar{n}_{hom} corresponds to the density of particles of the reference homogeneous system (i.e., with $V_i = 0$).

IV. NUMERICAL RESULTS

We choose the chemical potential $\mu = U/2$ such that the homogeneous system is at half-filling i.e. $\bar{n} = 1$. In all cases the hopping amplitude $t_{ij} = t$ is only between nearest neighbors. We set $t = 1$ to define the energy units and set the lattice constant $a = 1$ to define the length units in our numerical calculations. The band-width W of the system is given by $W = 2zt$, where z is the co-ordination number. The system is subjected to the periodic boundary conditions with a finite number of the lattice sites N_L . We perform our simulations at a zero temperature ($T = 0$).

The strength of electronic correlation is parametrized by tuning the parameter U . We study the 2d homogeneous system for different U values and see that the Mott transition occurs at $U_c \approx 11.5t$. Hence, we choose $U = 0t, 2t, 5t$, and $12t$ to represent a non-interacting lattice gas, a weakly interacting metallic phase, an intermediate interacting metallic phase, and a Mott insulating phase of the inhomogeneous system, respectively.

A. Two impurities

We start with the case where two impurities are present in the system. In Fig. 6 we show the interference patterns in FO due to two impurities of equal magnitude $V_{01} = V_{02} = 24t$ placed in the lattice sites $(15a, 15a)$ and $(15a, 22a)$ along a vertical direction of the square lattice for the non-interacting system and the interacting system with $U = 2t, 5t$, and $12t$. We further compare it with the case where only a single impurity is present in the system in Fig. 7. On comparing Fig. 6 and Fig. 7 the interference effect induced by the second impurity is visible. We see that within the HSEA the interaction does not change the position of the interference maxima and minima but reduce their heights and intensities

as seen in $U = 2t$ and $5t$ cases. This is analogous to the damping of FO with the interactions in the single impurity case. The behavior of the non-interacting system and the weakly-interacting one with $U = 2t$ is very similar. No interference effects and FO are visible in the Mott insulating phase at $U = 12t$.

In order to investigate how the interference maximum and minimum changes as we vary the relative distance between the impurities, in Fig. 8 we fix the position of the first impurity at $(15a, 15a)$ and vary the position of the second impurity to: $(15a, 19a)$, $(15a, 20a)$, $(15a, 21a)$, and $(15a, 27a)$. We show only the cases for $U = 2t$, and $5t$ since the behavior of the non-interacting system is very similar to the $U = 2t$ one and no interference effects are seen in the system with $U = 12t$. We see the occurrence of a minimum for $(15a, 19a)$, and a maximum for $(15a, 20a)$. Beyond a certain cross-over distance, e.g., for $(15a, 27a)$ the interference effects are negligible and the inhomogeneities behave independently as in the diluted impurity regime. Again, on comparing the cases $U = 2t$ and $U = 5t$ we see that the interaction does not change the position of the maximum and minimum but reduces their height. In other words, we conclude that the interaction reduces the interference effects.

We now place two impurities of equal magnitude $V_{01} = V_{02} = 24t$ along the diagonal direction of the lattice at sites $(10a, 10a)$ and $(15a, 15a)$ and show the cases for $U = 2t$, and $U = 5t$ in Fig. 9. Comparing Fig. 9 and Fig. 8 we already see that the interference patterns are qualitatively different when the impurities are placed along the diagonal. Particularly, for $U = 5t$ alternate regions of high and low density along the diagonal of the lattice are clearly visible. The interference pattern in the interstitial region between the two impurities is the most dominant. No FO or scattering interference effects are visible for $U = 12t$.

In order to get a quantitative description of the interference effects with the relative distance between the impurities we study the dependance of the screening charge as defined by Eq. (40) for different positions of the second impurity, i.e., when placed along the vertical or along diagonal directions as shown in Fig. 10 (top and bottom panels) respectively. When the two impurities are placed along the vertical line, an oscillatory behavior is seen in the screening charge, i.e., maxima (minima) appear when the impurities are separated by an odd (even) number of lattice sites both for the non-interacting and interacting systems. The screening charge does not change with distance and reaches its constant residual value in the Mott phase ($U = 12t$) again confirming the absence of any FO or interference effects in this regime.

The oscillatory behavior in screening charge with the distance is absent when the impurities are placed along the diagonal direction as seen in Fig. 10 (bottom panel). Along the diagonal direction the Manhattan distance

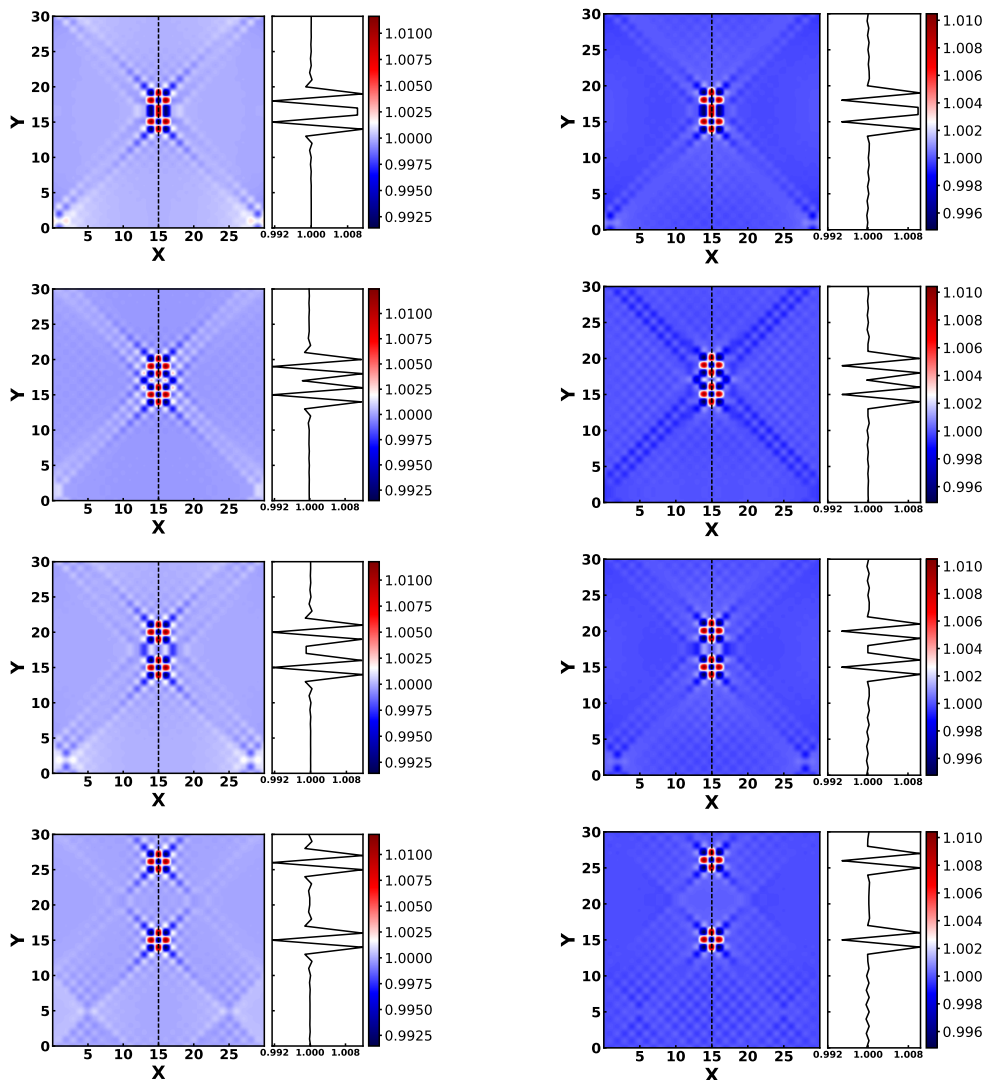


FIG. 8. The variation in the interference in the FO for different relative distances between the impurities. The first impurity V_{01} is kept fixed at $\vec{R}_{01} = (15a, 15a)$ and the position of the second impurity is shifted along the vertical line and placed at $\vec{R}_{02} = (15a, 19a)$, $\vec{R}_{02} = (15a, 20a)$, $\vec{R}_{02} = (15a, 21a)$, $\vec{R}_{02} = (15a, 27a)$ (from top to bottom). We show the interaction $U = 2t$ (left column), and $U = 5t$ (right column). All other model parameters, and the plotting style are the same as in Fig. 6.

between the two sites is always even and, hence, there are always interference minima in the FO. If one compares the evolution of Z for even lattice spacing in the upper panel with the same in the lower panel they almost match perfectly. The screening charge reaches the same constant residual value for $U = 12t$ like in the case when the impurities are placed along the vertical direction. In both cases, at any given distance the screening charge reduces with the increasing interactions, which is in agreement with the case when only a single impurity is present in the system [6].

B. Multiple impurities

We now move to a more complex case where we extend our studies to several impurities randomly scattered over

the surface. This aims to model a contaminated surface of a transition metal in the presence of dopant/defects, e.g. the Cr 001 surface in [13]. We use the square lattice, also to predict the behavior on the surfaces of 3d systems, exploiting the fact that lower dimensions can also mimic the higher dimensions in the DMFT approximation due to the momentum independence in the self-energy. This feature has also been exploited in [6].

In Fig. 11, we consider five impurities each of magnitude $V_0 = 10t$, randomly scattered over the lattice at sites: $(3a, 3a)$, $(20a, 5a)$, $(5a, 20a)$, $(25a, 22a)$, $(17a, 28a)$ for the non-interacting system and systems with $U = 2t$, $U = 5t$, and $U = 12t$. We see oscillations around the impurities together with a complex interference pattern (like a checkerboard) in the interstitial spaces between the impurities for the non-interacting system,

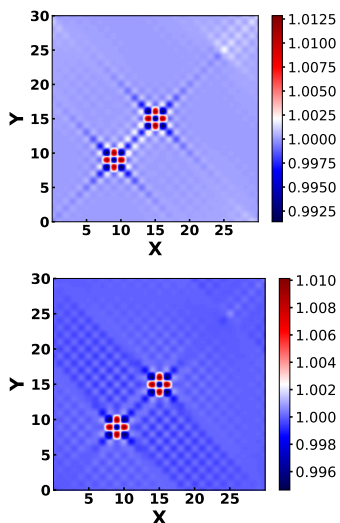


FIG. 9. Interference effect on FO due to the scattering from two impurities of equal magnitude, i.e., $V_{01} = V_{02} = 24t$, placed at $\vec{R}_{01} = (9a, 9a)$ and $\vec{R}_{02} = (15a, 15a)$, respectively, along the diagonal direction of the square lattice. We show the interactions $U = 2t$ (upper panel) and $U = 5t$ (lower panel). The model, all other parameters, and the plotting style are the same as in Fig. 6.

and systems with $U = 2t, 5t$. Interference effects get localized around the impurities with the increasing interactions (cf., $U = 5t$). No FO are observed in the Mott insulator for ($U = 12t$). This is in agreement to our previous studies where a single impurity or two impurities are present in the system. Thus we conclude that, at least within HSEA the absence of FO and any interference effects due to scattering in the Mott insulating phase is rather universal irrespective of the model of the inhomogeneous potential.

C. Extended inhomogeneity

We apply a step potential across the square lattice (32×32), i.e. for all the lattice sites with x-coordinates $X_i \leq 15a$ the potential is $V_0 = 3t$ and in the rest of the system is $V_0 = 0$. This potential models an extended inhomogeneity which could correspond to the surface irregularities in materials developed during the process of cleavage. In Fig. 12 we show local densities in the non-interacting system (upper panel) and in the interacting system with $U = 12t$ (middle panel). The step-like potential divides the lattice into two half-planes with a different average occupation (\bar{n}_i). FO is visible for $U = 0$, but the period of oscillations differ in the two half-planes as illustrated in the inset, where we show the FO in the cut perpendicular to the potential edge. Different oscillation periods originate from different uniform densities of particles in each halves of the systems. Any signature of FO is absent for the Mott phase ($U = 12t$), cf. the bottom panel of Fig. 12. In Fig. 12 (bottom panel) the influence of interactions in

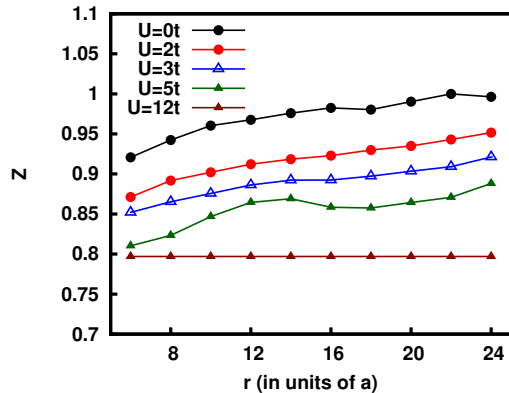
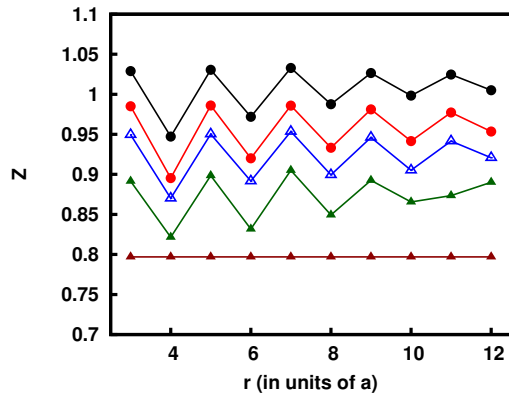


FIG. 10. Variation of the screening charge defined by Eq. (40) with relative (Manhattan) distance between the impurities ($V_{01} = V_{02} = 24t$). The impurities are placed in the vertical (diagonal) directions in the upper (lower) panel. Different values of the parameter U corresponds to the different interactions. We show $U = 0t, 2t, 5t$, and $12t$. The legends for the plot in the upper panel (not shown) is same as that of the lower panel.

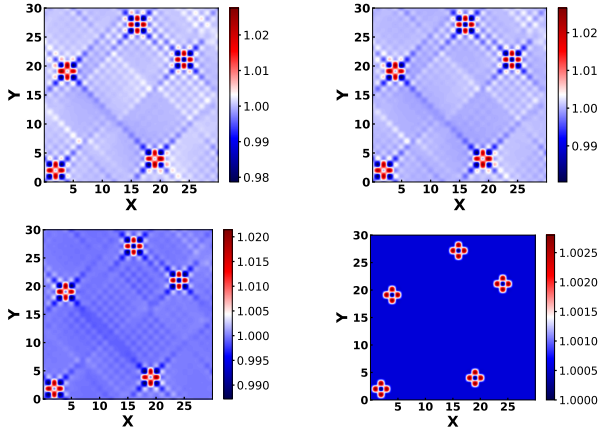


FIG. 11. Interference effect and FO in the presence of five impurities each of magnitude $V_1 = V_2 = V_3 = V_4 = V_5 = 10t$ randomly scattered over the lattice sites located at: $\vec{R} = (3a, 3a), (20a, 5a), (5a, 20a), (25a, 22a),$ and $(17a, 28a)$ of the square lattice. We show the non-interacting system and the system with the interactions $U = 2t$ (upper panel, left to right), and $U = 5t, U = 12t$ (lower panel, left to right). All other model parameters and the plotting style are the same as in Fig. 6.

this system is studied taking cuts perpendicular to the step of the potential. We see that the system becomes more homogeneous and the screening charge decreases with the increasing interaction.

D. A chain of impurities

Finally, we study the case where a chain of impurities each of magnitude ($V_0 = 24t$) is placed along the diagonal direction and a vertical direction of the square (31×31) lattice. This aims to model a domain wall or an interface. We investigate the behavior of FO for these two orientations of the chain with the different interactions. First, in Fig. 13 we present the case for the diagonally oriented chain for the non-interacting system and systems with $U = 2t, 5t,$ and $12t$. The insets show a projection of the densities along a zigzag line oriented perpendicularly to the diagonal direction. FO are visible around the chain and the behavior is similar for the non-interacting system and $U = 2t$, like in the other previous cases. FO get localized around the chain with the increasing interaction (cf., $U = 5t$). On the ends of the cut (corners of the lattice) we observe an increase of oscillations, which is due to the imposed periodic boundary conditions. In the case of a Mott insulator with $U = 12t$ no FO are visible. The chain creates an interface and effectively forms two subsystems separated in space.

In Fig. 14 we show the behavior for the system with the interactions if the chain of impurities is oriented along the vertical direction. The inset shows a horizontal cut perpendicular to the chain. In contrast, to the

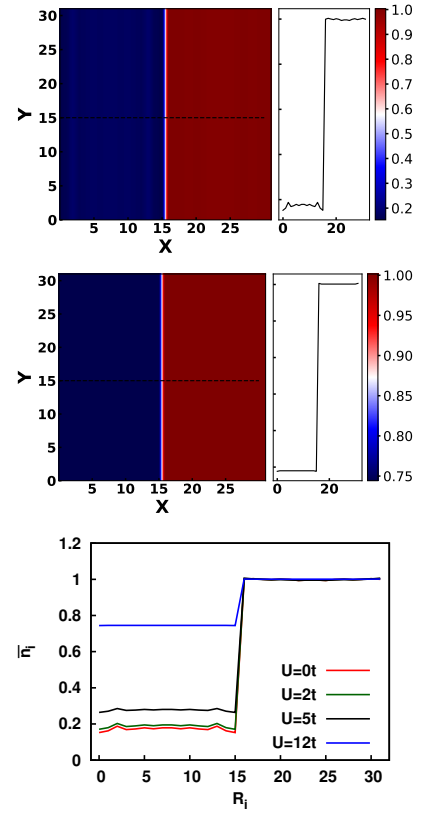


FIG. 12. Interference effect on FO due to the scattering from an extended inhomogeneity: A step potential applied across the square lattice (32×32), such that for all the lattice sites upto $(15a, 15a)$ $V_0 = 3t$ and $V_0 = 0$, otherwise. We show the non-interacting case (upper panel) and Mott phase ($U = 12t$) (middle panel). The right insets show oscillations on a cut (dotted line in the main panels) perpendicular to the step of the potential. In the bottom panel we compare a similar cut for the different interactions $U = 0t, 2t, 5t,$ and $12t$.

previous case we do not see any FO but just a density minimum corresponding to the repulsive potential both for the non-interacting and interacting systems. We only show the cases for $U = 2t$ and $U = 12t$ since the behavior of the system do not change much with the interactions. This different behavior as compared to the diagonally oriented chain lies in the geometrical orientation of the impurities with respect to each other. If the chain is vertically oriented, each impurity site has two neighboring sites occupied by the impurities. On the other hand, if the chain is diagonally oriented, each impurity site is completely surrounded by nearest neighboring sites without impurities. Hence, in the last case the distance between the impurity sites and the sites on a perpendicular cut, measured in Manhattan metric, is always even, in contrast to the former case, where it is always odd. This difference makes the interference pattern between FO created by each impurity from the chain always constructive in the diagonal case, while it is destructive in the vertical case.

In Fig. 15 we compare the FO from the diagonally ori-

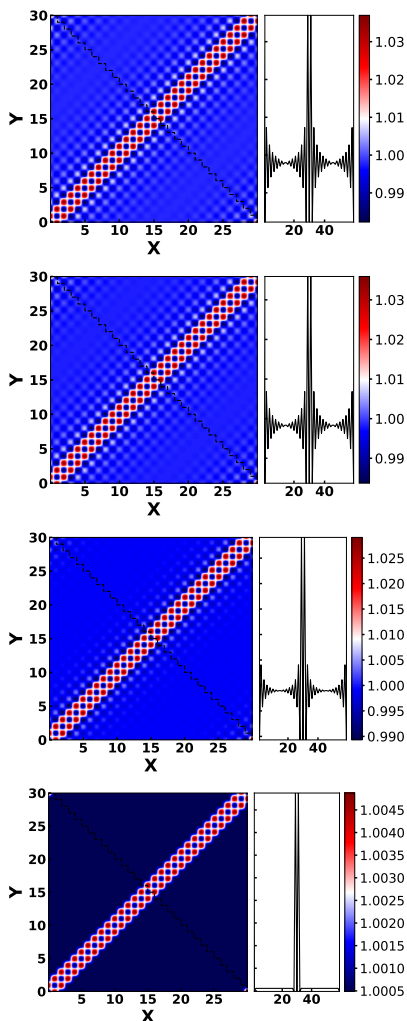


FIG. 13. Interference effect on FO due to the scattering from a chain of impurity atoms of equal magnitude $V_0 = 24t$ along the diagonal direction of the square lattice. The interaction parameter is $U = 0t, 2t, 5t,$ and $12t$ from the top to the bottom panel, respectively. The model, all other parameters, and the plotting style are the same as in Fig. 6.

ented chain (blue line) and from the vertically oriented chain (green line) of impurities, presented above, with the FO of a one-dimensional lattice having a single impurity potential (red line), with $N_L = 32$ sites and a single impurity $V_0 = 12t$ placed in the center. We also show the FO from a single impurity potential in the square lattice (black line). We consider the non-interacting systems for all these cases. The comparison shows that none of the 2d systems could be simplified to an assembly of 1d chains with a single impurity potential. While the vertically oriented chain shows no oscillations, the decay of FO due to the diagonally oriented chain is not exactly similar to the 1d chain. Eventually, the FO from both the vertically and diagonally oriented chains are also quite different compared to a chain from a 2d lattice with a single impurity potential at the center. Hence, the substantial role of the geometrical orientation of the chain of impurities on the interference effect prevents

one to simplify this system to an equivalent 1d chains with single impurity potentials assembled together.

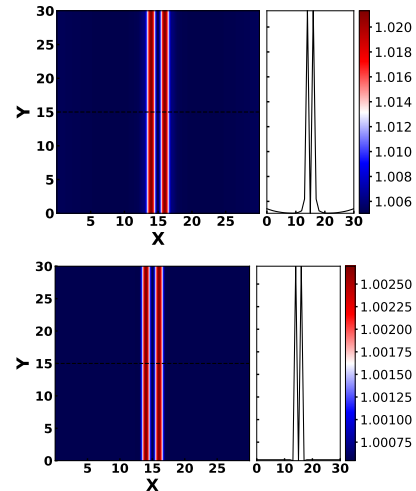


FIG. 14. Interference effect on FO due to the scattering from a chain of impurity atoms of equal magnitude $V_0 = 24t$ along the vertical line of the square lattice. The interaction parameter is $U = 2t,$ and $12t$ from the top to the bottom panel, respectively. The model, all other parameters, and the plotting style are the same as in Fig. 6.

V. CONCLUSIONS

We have studied the interference effects in FO due to the scattering from two impurities, multiple impurities, extended inhomogeneities in non-interacting and interacting fermion systems. On comparing the FO in the presence of a single impurity we see that in two impurity systems, the additional impurity induces interference effects on FO. The interference maxima and minima change with the relative position of the impurities up to a certain cross-over distance beyond which the impurities behave independently. The interaction does not change the position of maxima and minima but reduces their intensity and consequently the interference effects. The screening charge shows an oscillatory behavior with the even and odd lattice spacing between the impurities along a vertical column. A more complex pattern is seen in the presence of multiple impurities but the FO still localize around the impurities with the increasing interactions. In case of the extended inhomogeneities the system becomes more homogeneous with the increasing interactions. In case of a chain of impurities in the square lattice FO is present for a diagonal chain while absent for a vertical chain due to constructive and destructive of FO in these two geometries respectively. In all the models of the impurity potential no FO or interference effects are seen in the Mott insulating phase.

For a completeness we also presented a theory of FO in non-interacting fermions in an empty space with

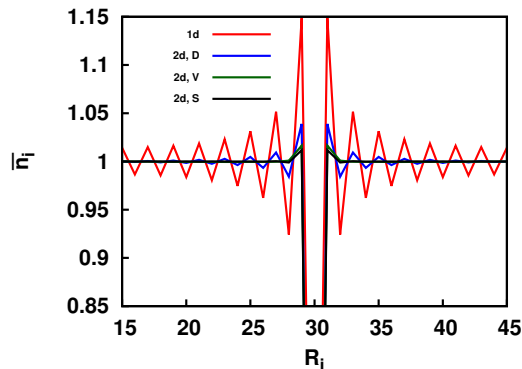


FIG. 15. Comparison of FO along: 1d lattice chain with $N_L = 32$ sites and a single impurity potential $V_0 = 12t$ placed at the center (1d), across the perpendicular cut for a chain of impurities $V_0 = 24t$ along the diagonal chain (D), vertical chain (V), and a single impurity potential $V_0 = 24t$ placed at the centre of the square lattice (S). We show the non-interacting case $U = 0t$.

localized impurities. The exact analytical formulation was derived and generalization of the Friedel formula was obtained within the independent impurities approximation. A few numerical results in two and three dimensional systems were given.

We have used a homogeneous self-energy approximation based on DMFT for our studies where the inhomogeneous part of the self-energy due to the contribution from the impurities is neglected. Probing the additional effects on the interference in FO when we calculate the full self-energy solving the R-DMFT equations self-consistently or include the spatial correlation effects beyond the single-site DMFT would give a more complete picture on top of our studies. Still, in order to establish a connection with the real materials, the model is rather simplistic. One needs to further extend such studies using the material specific DMFT (LDA+DMFT) solving the multi-band Hubbard model. Our work can be a good starting point to motivate such realistic modeling and future experiments.

ACKNOWLEDGMENTS

This work was supported by Foundation for Polish Science (FNP) through the TEAM/2010-6/2 project, co-financed by the EU European Regional Development Fund. We thank D. Vollhardt for motivating discussions. BC acknowledges discussions with J. Kolorenč, and V. Pokorný. Computing facilities provided by the Czech National Grid Infrastructure MetaCentrum (project CES-NET LM2015042) is gratefully acknowledged.

-
- [1] J. Friedel, *Phil. Mag.* **43**, 153 (1952).
 - [2] J. Friedel, *Nuovo Cimento Supp.* **7**, 287 (1958).
 - [3] H. Alloul, *J. Supercond. Nov. Magn.* **25**, 585 (2012).
 - [4] B. Chatterjee and K. Byczuk, *J. Phys.: Conf. Ser.* **592**, 012059 (2015).
 - [5] K. Byczuk, B. Chatterjee, D. Vollhardt *Euro. Phys. J. B* **92**, 23 (2019).
 - [6] B. Chatterjee, J. Skolimowski, K. Makuch, K. Byczuk *Phys. Rev. B* **100**, 115118 (2019).
 - [7] M. F. Crommie, C. P. Lutz, and D. M. Eigler, *Science* **262**, 218 (1993).
 - [8] D. M. Eigler and E. K. Schweizer, *Nature (London)* **344**, 524 (1990).
 - [9] K. Kanisawa, M. Butcher, H. Yamaguchi, and Y. Hiramaya, *Phys. Rev. Lett* **86**, 3384 (2001).
 - [10] G. Binnig, H. Rohrer, Ch. Gerber, and E. Weibel, *Appl. Phys. Lett.* **40**, 178 (1982); *Phys. Rev. Lett.* **49**, 57 (1982); *ibid.* **50**, 120 (1983).
 - [11] K. W. Clark, X-G. Zhang, G. Gu, J. Park, G. He, R. M. Feenstra, and A.-P. Li, *Phys. Rev. X* **4**, 011021 (2014).
 - [12] Chico L et. al, *Acta Phys. Pol. A*, **114** (2008).
 - [13] O. Y. Kolesnychenko, G. M. M. Heijnen, A. K. Zhuravlev, R. de Kort, M. I. Katsnelson, A. I. Lichtenstein, H. van Kempen, *Phys. Rev. B* **72**, 085456 (2005).
 - [14] R. Egger, and H. Grabert, *Phys. Rev. Lett* **75**, 3505 (1995).
 - [15] C. Schuster, and P. Brune, *Phys. Status Solidi B* **241**, 2043–2054 (2004).
 - [16] D. Vieira, H. J. P. Freire, V. L. Campo Jr, and K. Capelle, *J. Magn. Magn.* **320**, e418–e420 (2008).
 - [17] G. E. Simion, and G. F. Giuliani, *Phys. Rev. B* **72**, 045127 (2005).
 - [18] W. Ziegler, H. Endres, and W. Hanke, *Phys. Rev. B* **58**, 4362 (1998).
 - [19] I. Affleck, L. Borda, and H. Saleur, *Phys. Rev. B* **77**, 180404 (2008).
 - [20] D. Vollhardt, K. Byczuk, and M. Kollar, in *Strongly Correlated Systems*, ed. by A. Avella and F. Mancini, p. 203 (Springer, 2012).
 - [21] D. Vollhardt, A. Avella, and F. Mancini, *AIP Conference Proceedings* **1297**, 339 (2010).
 - [22] D. Vollhardt, *Correlated Electron Systems* **57** (1993).
 - [23] G. Kotliar, and D. Vollhardt, *Phys. Today* **57**, 53 (2004).
 - [24] K. Byczuk, in *Condensed Matter Physics In The Prime Of The 21st Century: Phenomena, Materials, Ideas, Methods*, ed. by Janusz Jędrzejewski, pp. 1-33 (World Scientific, 2008).
 - [25] I. Titvinidze, A. Schwabe, N. Rother, and M. Potthoff, *Phys. Rev. B* **86**, 075141 (2012).
 - [26] V. I. Anisimov, A. I. Poteryaev, M. A. Korotin, A. O. Anokhin, and G. Kotliar, *J. Phys. Condens* **9**, 7359 (1997).

- [27] R. W. Helmes, T. Costi, and A. Rosch, Phys. Rev. Lett. **100**, 056403 (2008); *ibid.* **101**, 066802 (2008).
- [28] M. Snoek, I. Titvinidze, C. Toke, K. Byczuk, and W. Hofstetter, New J. Phys. **10** 093008 (2008).
- [29] M. Y. Suárez-Villagrán, N. Mitsakos, T. H. Lee, V. Dobrosavljević, J. H. Miller, Jr, E. Miranda, E, Phys. Rev. B **101**, 235112 (2020).
- [30] J. K. Freericks, *Transport in Multilayered Nanostructures: The Dynamical Mean-field Theory Approach*, (Imperial College Press, 2006).
- [31] I. Grosu, and L. Tugulan, J. Supercond. Nov. Magn **21**, 65 (2008).
- [32] Y. L. Liu, Phys. Rev. B **68**, 155116 (2003).
- [33] P. G. Derry, A. K. Mitchell, D. E. Logan, Phys. Rev. B **92**, 035126 (2015).
- [34] A. K. Mitchell, P. G. Derry, Andrew K D. E. Logan, Phys. Rev. B **91**, 235127 (2015).
- [35] M. Schüler, S. Barthel, M. Karolak, A. I. Poteryaev, A. I. Lichtenstein, M. I. Katsnelson, G. Sangiovanni, and T. O. Wehling, Phys. Rev. B **93**, 195115 (2016).
- [36] J. Kolorenč, A. B. Shick, and A. I. Lichtenstein Phys. Rev. B **92**, 085125 (2015).
- [37] D. J. Choi, C. R. Verdú, J. de Bruijckere, M. M. Ugeda, N. Lorente, and J. I. Pascual, Nat. Comm. B **8**, 1 (2017).
- [38] E. N. Economou, *Green's Functions in Quantum Physics*, Springer Series in Solid-State Sciences (Springer-Verlag, Berlin, Hiedelberg, 2006).
- [39] E. Fermi, Ric. Sci. **7**, 13 (1936).
- [40] K. Wódkiewicz, Phys. Rev. A **43**, 68 (1991).
- [41] B. Donner, M. Kleber, C. Bracher, and H. J. Kreuzer, Am. J. Phys. **73**, 690 (2005).
- [42] T. T. Le, Z. Osman, D. K. Watson, M. Dunn, and B. A. McKinney, Phys. Scripta **94**, 065203 (2019).
- [43] F. García-Moliner, *Quantum-mechanical techniques*, in *Theory of imperfect crystalline solids: Trieste lectures 1970*, pp. 1-100 (International atomic energy agency, Vienna 1971).
- [44] J. Hubbard, Proceedings of the Royal Society of London A: Mathematical, Physical and Engineering Sciences **276**, 238 (1963).
- [45] M. C. Gutzwiller, Phys. Rev. Lett. **10**, 159 (1963).
- [46] J. Kanamori, Prog. Theor. Phys. **30**, 275 (1963).
- [47] G. Rickayzen, *Green's functions and condensed matter*, (London; New York Academic Press, 1980).
- [48] R. Bulla, Phys. Rev. Lett. **83**, 136 (1999).
- [49] R. Žitko, www.nrgljublana.ijs.si (2014).
- [50] T. A. Costi, and A. Hewson, Physica B: Cond Matt **163**, 179 (1990).